

# Self-Supervised Video Representation Learning in a Heuristic Decoupled Perspective

Zeen Song, Jingyao Wang, Jianqi Zhang, Changwen Zheng, Wenwen Qiang

## ABSTRACT

Video contrastive learning (v-CL) has gained prominence as a leading framework for unsupervised video representation learning, showcasing impressive performance across various tasks such as action classification and detection. In the field of video representation learning, a feature extractor should ideally capture both static and dynamic semantics. However, our series of experiments reveals that existing v-CL methods predominantly capture static semantics, with limited capturing of dynamic semantics. Through causal analysis, we identify the root cause: the v-CL objective lacks explicit modeling of dynamic features and the measurement of dynamic similarity is confounded by static semantics, while the measurement of static similarity is confounded by dynamic semantics. In response, we propose *Bi-level Optimization of Learning Dynamic with Decoupling and Intervention* (BOLD-DI) to capture both static and dynamic semantics in a decoupled manner. Our method can be seamlessly integrated into the existing v-CL methods and experimental results highlight the significant improvements.

## CCS CONCEPTS

• Computing methodologies → Computer vision representations.

## KEYWORDS

Video representation learning, Video contrastive learning, Self-supervised learning

## 1 INTRODUCTION

Extracting informative features from large-scale video data in the absence of label information presents a challenging task [14, 34, 44, 49]. In recent years, contrastive learning has achieved significant success in image representation learning [1, 8, 22, 26, 71]. Building on this progress, researchers have extended it to the domain of video data, resulting in the emergence of video contrastive learning (v-CL) methods with impressive results in downstream tasks such as action classification [44] and action detection [23].

Existing v-CL methods [14], e.g., v-SimCLR [8], v-BYOL [22], v-MoCo [26], and CVRL [44], treat augmented clips from the same video as positive samples and clips from different videos as negative samples. However, in the training phase, these methods constrain the feature representations of positive samples to be similar based on cos distance/L2 distance [8, 26]. Empirically, this similarity measurement cannot reveal the temporal information contained in the

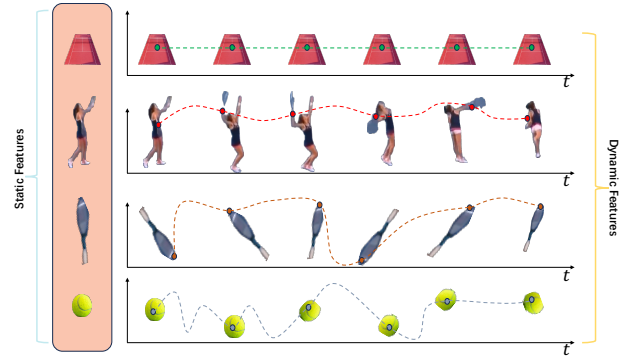


Figure 1: Visualization of static and dynamic semantics from a video capturing a tennis match.

samples, which makes it difficult for the feature extractor learned by v-CL to mine the important dynamic semantics in the videos.

To this end, we conduct a series of exploratory experiments to explore whether v-CL can learn the true temporal dynamic from large-scale unannotated video data. More details are provided in Section 3.2. Specifically, we first individually pre-train a Slow-only R-50 network [13] and a classifier on Kinetics-400 [31] for each v-CL method, i.e., v-SimCLR, v-MoCo, and v-BYOL [14]. In the first experiment, we freeze all the parameters and calculate the accuracy when changing the input clips from real video clips into static video clips, i.e., the frames within each clip are all copies of the first frame. In the second experiment, we train a classifier based on the output of the feature extractor when the parameters of the feature extractor are frozen. Ideally, in the first experiment, the prediction performance of static clips should be significantly lower than that of real video clips, because there are no dynamic semantics in the static clips. In the second experiment, the classifier should be able to distinguish whether an input video clip is in the right temporal order or a randomly shuffled order. However, the experimental results in Subsection 3.2 show contradicting results. We observe that: (1) when the input video clips are static, the classification accuracy of v-CL methods is only slightly lower than that of normal video clips, which means the classification results in standard evaluation mostly depend on static semantics; and (2) the learned classifier can't correctly distinguish right-order video clips from random-order ones, which means the learned representation is incapable of classifying tasks that are static similar, but dynamic varies.

These observations suggest that the feature extractor extracts mostly static semantics and only a few dynamic semantics during the v-CL procedure. In contrastive learning, the feature extractor learns the invariant features between positive pairs [60] by measuring the similarity between samples, i.e., maximizing the similarity between positive sample pairs and minimizing the similarity between negative sample pairs. Through causal analysis in Subsection

3.3, we discover the confounding effect in the representation learning process of v-CL, where static semantics confound the learning of dynamic semantics and dynamic semantics confound the learning of static semantics. This motivates us to learn static and dynamic semantics in a decoupled manner.

To address this issue, we introduce BOLD-DI, a novel bi-level optimization approach detailed in Section 4, designed to extract both static and dynamic semantics in a decoupled manner. BOLD-DI is comprised of three key modules: the Dynamic Module, which models the dynamic semantics; the Stratify Module, which stratifies the dynamic semantics based on the learned representations; and the Static Module, which focuses on modeling the static semantics. The objective of BOLD-DI consists of two stages. In the first stage, we learn the static semantics by eliminating the confounded effect of dynamic semantics with the backdoor adjustment. In the second stage, conditioned on the first stage, the feature extractor extracts only dynamic semantics with the dynamic Module, and the v-CL objective then integrates both the learned static and dynamic semantics into a unified representation. Iterative updates of these two stages can help the feature extractor learn better static and dynamic features in a decoupled manner.

In Section 5, we empirically evaluate the effectiveness of our approach by evaluating the downstream performance on action recognition benchmark datasets, including Kinetics-400 [31], UCF-101 [52], and HMDB-51 [35]. We also evaluated our results on motion-aware datasets, i.e. Something-Something v2 [21] and FineGym [51]. Through extensive experiments on downstream tasks, we demonstrate that our proposed BOLD-DI provides significant improvements. Our contributions are as follows.

- We conduct a series of experiments and observe that the representation learned through current v-CL methods contains mostly static semantics rather than dynamic semantics. Through causal analysis, we discover the confounding effect of static semantics when learning dynamic semantics, and also the confounding effect of dynamic semantics when learning static semantics. This motivates us to learn both static and dynamic semantics in a decoupled manner.
- We propose *Bi-level Optimization of Learning Dynamic with Decoupling and Intervention* (BOLD-DI), a bi-level optimization method that can learn both the static and dynamic semantics well in a decoupled manner, eliminating the confounding effect when measuring similarity between samples.
- Extensive experiments conducted on various benchmark datasets demonstrate our method’s superiority for both action classification and detection tasks and show significant improvement compared to the original v-CL methods. Ablation studies further affirm the effectiveness of our approach.

## 2 RELATED WORKS

**Self-Supervised Video Representation Learning.** With the success of image self-supervised learning [8, 22, 25, 26], the video self-supervised learning (VSSL) has become popular in recent years [14, 15, 44, 58, 64]. The VSSL methods can be divided into two types, i.e., pretext-learning-based and v-CL-based methods.

The pretext-learning-based methods utilize pretext learning tasks such as predict rotation [16, 28, 30, 62], predict optical flow [62],

classify playback speed [2] and classify temporal order [16] to learn representations that are useful for downstream tasks.

The v-CL-based methods [14, 44] mainly construct positive, i.e., different clips from the same video, and negative sample pairs, i.e., clips from different videos, using various data augmentation techniques [14, 32, 44, 47], thereby increasing the similarity between the representation of positive pairs and decreasing the similarity between the representation of negative pairs.

In this paper, through a series of experiments, we find that current v-CL methods primarily extract static semantics, with only limited dynamic semantics being captured. Moreover, through causal analysis, we reveal that the main reason for this phenomenon lies in the confounding effects of static semantics during the measurement of dynamic similarity. Therefore, in our method, we explicitly model the dynamic semantics during the feature extraction process in the Dynamic Module.

### Explicitly model dynamic in video representation learning.

In the field of video representation learning, an important issue is how to capture the dynamic semantic information of videos.

Within the pretext-learning-based approach, researchers have designed various pretext tasks to help the feature extractor distinguish different dynamic information within video content. Specifically, SpeedNet [2] is trained to predict the “speediness” of moving objects in videos. PacePred [63] is trained to recognize the paces of clips and it also involves context-based contrastive objective to learn the appearance features of videos. VTHCL [67] is trained to maximize the mutual information between slow and fast videos.

Within the v-CL methods, the key to making the feature extractor capture the dynamic semantics of videos lies in how to establish positive and negative sample pairs, so that representations of clips with similar dynamic information are similar, while representations of clips with different dynamic information are dissimilar. Specifically, CoCLR [24] and MaCLR [65] treat RGB frames and optical flows of the same video clip as positive sample pairs.

Seco [69] and DSM [61] both use correctly ordered video clips as positive sample pairs and incorrectly ordered clips as negative sample pairs.

In this paper, contrary to previous approaches, we argue that including only dynamic information in video representation learning is also limited. Through causal analysis, we reveal that dynamic semantics can also lead to confounding effects when measuring static similarity, hindering the learning of static semantics. Based on these analyses, we propose a novel algorithm to learn static and dynamic semantics in a decoupled manner, avoiding the feature extractor to merely learn static or dynamic features.

## 3 PROBLEM ANALYSIS

In this section, we first briefly introduce common approaches in v-CL. Subsequently, through a series of experiments, we observe: v-CL methods mostly extract static features, with only a minimal inclusion of dynamic features. We employ a Structure Causal Model (SCM) to illustrate that the primary reason behind v-CL’s limited ability to capture dynamic features lies in the confounding influence of static semantics on the measurement of dynamic similarity.

### 3.1 Preliminary

We start by first introducing the common approaches in v-CL. Given a mini-batch of videos  $\{X_i = \{x_{i,t}\}_{t=1}^T\}_{i=1}^N$  sampled from the dataset, where  $x_{i,t} \in \mathbb{R}^{H \times W \times C}$  represents each frame in this clip,  $N$  represents the batch size,  $T$  represents the number of frames inside a video and  $H, W, C$  represent the height, the width and the number of channels of the frame. Each clip  $X_i$  is applied with augmentations  $\rho_j$  for  $\varrho$  times to get  $\varrho$  positive samples,  $j \in \{1, \dots, \varrho\}$ . The augmentation  $\rho_j$  includes both temporal and spatial augmentations. The temporal augmentation randomly samples video clips with length  $L$  and a stride of  $\delta$ . The spatial augmentation is temporal consistent [14, 44], which means applying the same augmentation such as cropping, color distortion, and random horizontal flip [57] to each frame inside a clip. The spatiotemporal feature extractor  $f_\theta$  then takes  $X_i$  as the input and outputs an embedding  $Z_i$  for each clip. For each augmented video clip  $\rho_j(X_i)$ , when it is regarded as the anchor, contrastive learning aims to maximize the similarity between it and positive samples, i.e., the video clip  $\rho_k(X_i)$ ,  $k \in \{1, \dots, \varrho\}$ ,  $k \neq j$ , from the same video  $X_i$ . Augmented video clips that are generated by  $X_j$ ,  $j \neq i$ , are treated as negative samples. We denote the  $Z_+$  as the set of embeddings of positive samples and  $Z_-$  as the set of embeddings of negative samples for embedding  $f_\theta(\rho_j(X_i))$ . The objective for each clip is InfoNCE [40]:

$$\ell_{i,j}^\rho = -\log \frac{\sum_{Z_+} \exp(\text{sim}(f_\theta(\rho_j(X_i)), Z_+)/\alpha)}{\sum_{Z \in \{Z_+, Z_-\}} \exp(\text{sim}(f_\theta(\rho_j(X_i)), Z)/\alpha)}, \quad (1)$$

where  $\alpha$  is a temperature hyper-parameter. v-SimCLR [8] uses the embeddings of clips of other videos within the minibatch as the set of negative samples  $Z_-$ . v-MoCo [26] uses the online network  $f_\theta$  to encode the positive samples while using the target network  $f_{\theta_m}$  to encode the negative samples. The parameters  $\theta_m$  are updated with a moving average  $\theta_m \leftarrow \gamma\theta_m + (1-\gamma)\theta$ , where  $\gamma$  is a hyper-parameter, instead of direct back-propagation. The negative embeddings  $Z_-$  are taken from a queue that stores embeddings of clips from previous iterations. v-BYOL [22] uses the same structure as v-MoCo but with an extra predictor  $f_{\theta_p}$ . v-BYOL does not use negative samples, and the objective is

$$\ell_{i,j}^\rho = \sum_{Z_+} \text{sim}(f_\theta(\rho_j(X_i)), Z_+). \quad (2)$$

We use  $\mathcal{L}_{cl} = \sum_i^N \sum_j^{\varrho} \ell_{i,j}^\rho$  to denote the video contrastive loss of the videos in a mini-batch.

### 3.2 Empirical Analysis

In video representation learning, a proficient feature extractor should efficiently capture both static and dynamic semantics. Static semantics can be regarded as related to physical entities, such as the tennis court, racket, and ball in a tennis video [3]. On the other hand, dynamic semantics are related to the temporal changes in entities within the video. For instance, in the context of playing tennis, dynamic semantics involve the individual movement trajectories of the tennis player, the tennis racket, and the tennis ball, as illustrated in Figure 1.

To investigate the effectiveness of feature extractors in capturing dynamic features within video self-supervised learning, we conduct a series of experiments. During pre-training, we individually

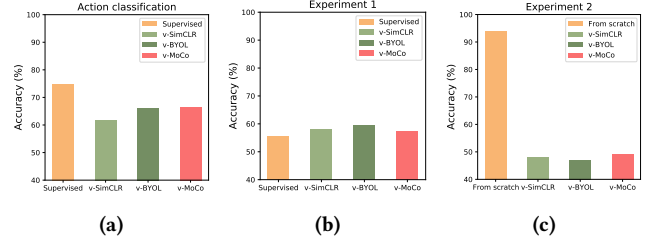


**Figure 2: Experimental results of Subsection 3.2. (a) The standard linear evaluation results on the Kinetics400 dataset for v-CL methods and supervised method. (b) The linear evaluation results when the input clips are switched to static video clips. (c) The classification accuracy, where the weights of the feature extractor are frozen and a classifier is trained to distinguish right-order clips from random-shuffled clips.**

employ the v-SimCLR, v-MoCo, and v-BYOL methods [14]. The pre-training utilizes the Kinetics-400 dataset [31], employing the Slow-only R50 model [13] as the backbone network. We use clip length  $L = 8$ , a stride  $\delta = 8$ , and  $\varrho = 2$  positive samples sampled from the same video.

We perform two distinct experiments: (1) We maintain the feature extractor and classifier unchanged, transforming the video clips used for evaluation from 8x8 video clips to copies of the first frame image, followed by calculating classification accuracy. (2) We deliberately disrupt the temporal order of video clips to investigate the capability of capturing dynamic features. With the feature extractor fixed, we train a classifier to distinguish between the shuffled video clips and the correctly ordered ones. For comparison, we also report the accuracy of action classification trained with the supervised method and the accuracy of supervised training from scratch in the second experiment.

The experimental results are presented in Figure 2. From the results, we can obtain the following observations: (1) When static video clips are utilized as input for feature extractors learned through v-CL, their classification accuracy is only marginally lower than that achieved using normal video clips for classification. (2) The classification accuracy of v-CL methods is notably lower than that of feature extractors trained through supervised learning. (3) Classifiers encounter challenges in effectively distinguishing disordered video sequences from correct sequenced ones when feature extractors learned through v-CL are applied. (4) Interestingly, the feature extractor, with the same network structure, demonstrates an ability to distinguish disordered video sequences from ordered ones when it is trained from scratch using supervised learning.

Observations (1) and (3) suggest that in v-CL, the feature extractor predominantly captures static features, with only a limited extraction of dynamic features. Meanwhile, observations (2) and (4) highlight that the ability to capture dynamic features is closely tied to the optimization objective. This prompts us to conduct an in-depth analysis of v-CL’s objective in the subsequent subsection.

### 3.3 Causal Analysis

The objectives of v-CL are designed to learn features by measuring the similarity between samples. In this paper, we employ a Structure Causal Model (SCM) [43] to provide a detailed explanation on the

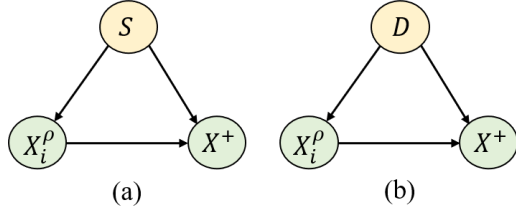


**Figure 3: The structural causal model.**  $X_i^\rho$  and  $X^+$  represent the video clips of the anchor sample and one of the rest samples.  $S$  is the static semantics,  $D$  is the dynamic semantics.

measurement process. In SCM, a directed acyclic graph (DAG) is employed to depict relationships among causal variables, where nodes represent causal variables, and the edge  $X \rightarrow Y$  indicates that variable  $X$  is a cause of variable  $Y$ .

Figure 3(a) is to illustrate the learning process of dynamic semantics. The premise to achieve the purpose of learning dynamic semantics is that the similarity between the other samples and the anchor should be calculated based on the dynamic semantics in Figure 3(a). Specifically,  $X^+$  and  $X_i^\rho$  represent the video clips of the anchor sample and one of the rest sample, respectively. The variable  $S$  denotes shared static semantics. The edge  $X_i^\rho \rightarrow X^+$  symbolizes dynamic similarity between two samples. According to [43], we can obtain that  $X_i^\rho \leftarrow S \rightarrow X^+$  is a crotch-structure, which implies that shared static semantics confound the measurements of dynamic similarity. This confounding effect arises from the fact that in Equation (1) and Equation (2),  $Z$  contains both static and dynamic features, with no guarantee as to which part of  $Z$  contains dynamic features. Consequently, the similarity measure between dynamic semantics between samples receives the confounding of static semantics, e.g., the measurement of dynamic similarity between different samples is not solely due to  $X_i^\rho \rightarrow X^+$  but is also influenced by spurious correlations through  $X_i^\rho \leftarrow S \rightarrow X^+$ . This can lead to inaccuracies in the semantics of the dynamics learned. Meanwhile, implementing a similar analysis to that described above for Figure 3(b), we can obtain that the similarity measure between dynamic semantics between samples receives the confounding of static semantics, e.g., the measurement of static similarity between different samples is not solely due to  $X_i^\rho \rightarrow X^+$  but is also influenced by spurious correlations through  $X_i^\rho \leftarrow D \rightarrow X^+$ . This can lead to inaccuracies in the semantics of the statics learned.

In conclusion, we can obtain through causal analysis that when learning static semantics, dynamic semantics interferes with its learning process and vice versa. Meanwhile, we give that the main reason for this phenomenon is that the feature extractor has no way to decouple the static and dynamic semantics in the learning process. Therefore this motivates us to propose in this paper a v-CL from the decoupling perspective.

## 4 METHOD

To guide v-CL in simultaneously capturing static and dynamic features, we propose *Bi-level Optimization of Learning Dynamic with Decoupling and Intervention* (BOLD-DI). It comprises three modules, including (1) The Dynamic Module, which explicitly models dynamic semantics during the feature extraction process. (2) The Stratify Module, which stratifies dynamic semantics based

on learned representation. (3) The Static Module, which explicitly models static semantics during the feature extraction process.

### 4.1 Dynamic Module

In this subsection, we introduce the proposed dynamic module, which aims to empower the feature extractor obtained from v-CL to precisely mine dynamic semantics in video samples. We start by considering the video as a discrete dynamic system, which can be presented as follows:

$$x_{t+1} = F(x_t, t), x \in \mathcal{X}, \quad (3)$$

where  $\mathcal{X}$  is the space of video frames, and  $F(x, t)$  is the transition function governing the update rule for each frame  $x$  at timestep  $t$ . The closed-form solution of Equation (3) enables the generation of the future frames given the history frames. In other words, this solution explicitly depicts the dynamic change relationship between the front and back frames in a video clip, which is the key to capturing dynamic semantics.

In most cases, the  $F$  in Equation (3) is nonlinear [38], making it impractical to obtain a closed-form solution from Equation (3). To address this challenge, Koopman theory [33] is proposed. The key idea is to learn a map  $\mathcal{G} : \mathcal{X} \rightarrow \mathcal{U}$  to transfer the nonlinear dynamic system into an infinite-dimensional space  $\mathcal{U}$ , in which the nonlinear dynamic system can be fully described by a linear Koopman operator  $\mathcal{K}$ :

$$\mathcal{K}\mathcal{G}(x_t) = \mathcal{G}(F(x_t)) = \mathcal{G}(x_{t+1}), \quad (4)$$

Due to the infinite-dimensional characterization, the Koopman operator is also difficult to implement in real scenarios. Then, data-driven methods [39, 50, 54] are presented to provide approximations of  $\mathcal{K}$  and  $\mathcal{G}$  in the finite-dimensional space.

Before introducing the dynamic module, let us revisit Equation (4) from a decoupling perspective. We can observe that the dynamic properties in Equation (4) are embedded in the process of modeling the changes between the current frame and the subsequent frame, and need to be given the  $\mathcal{G}$ . Meanwhile, the role of  $\mathcal{G}$  is to extract the semantics of individual frames in the sample. Thus, we can conclude that: 1) the  $\mathcal{G}$  in Equation (4) can be regarded as related to static semantic information, e.g., the semantics extracted from a single frame; 2) the  $\mathcal{K}$  in Equation (4) can be regarded as related to dynamic semantic information; 3) the dynamic semantic information can be regarded as extracted based on the static semantic information, e.g.,  $\mathcal{K}$  can be presented as  $\mathcal{G}(x_t)^{-1}\mathcal{G}(x_{t+1})$ .

Inspired by the above discussion, we now present our dynamic module. If we consider the feature extractor  $f_\theta$  to be  $\mathcal{G}$ , then the key to the dynamic module enabling the feature extractor to learn the dynamic semantics is that: 1) there exists a  $\mathcal{K}$  that can satisfy  $\mathcal{K}f_\theta(x_t) = f_\theta(x_{t+1})$ ; 2)  $\mathcal{K}$  is generated by  $f_\theta$ . This is because in Equation (4) the dynamic semantic information and the static semantic information are related to different components of Equation (4). However, in our scenario, the dynamic and static semantic information are all related to  $f_\theta$ . Based on [39, 50, 54], we can obtain that the Koopman operator can be obtained in a data-driven manner. Specifically, if  $f_\theta$  can extract all static semantics, we can denote the static-semantic-related representation of each frame as  $u_t = f_\theta(x_t)$ , and for each video clip  $X$ . Then, the corresponding static-semantic-related representations are given by

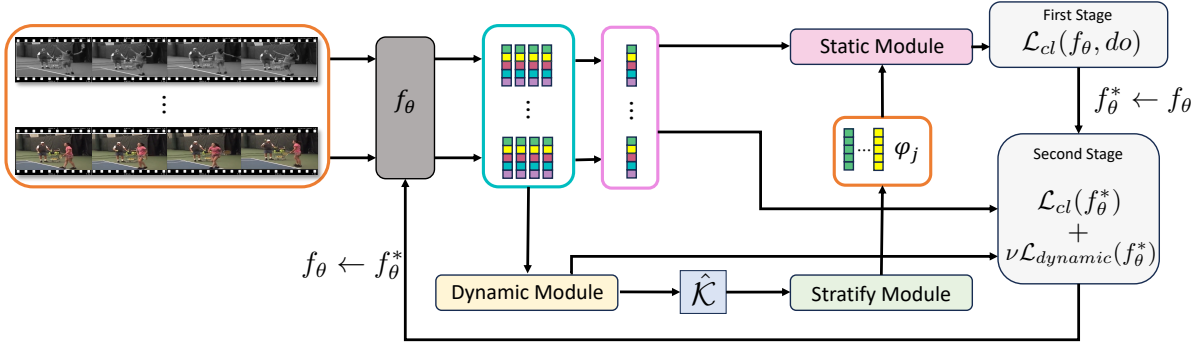


**Figure 4: The framework of BOLD-DI. The pipeline follows the standard v-CL procedures with three novel modules: Dynamic Module (Subsection 4.1), Stratify Module (Subsection 4.2), Static Module (Subsection 4.3).**

$U = [u_1, u_{1+\delta}, \dots, u_{1+(L-1)\delta}] \in \mathbb{R}^{M \times L}$ . Thus, the Koopman operator  $\hat{\mathcal{K}}$  can be estimated with:

$$\hat{\mathcal{K}} = U_{fore} U_{back}^\dagger, \quad (5)$$

where  $U_{fore} = [u_{1+\delta}, \dots, u_{1+(L-1)\delta}] \in \mathbb{R}^{M \times (L-1)}$ ,  $\dagger$  denotes the Moore-Penrose pseudoinverse, and  $U_{back} = [u_1, \dots, u_{1+(L-2)\delta}] \in \mathbb{R}^{M \times (L-1)}$ .

To this end, we present the learning process of dynamic semantics in  $f_\theta$  with the pre-given  $\hat{\mathcal{K}}$ . The key idea is that the predicted per-frame representation  $u_l$  should be able to predict the next frame with  $\hat{\mathcal{K}}$ . i.e.,  $f_\theta(x_{l+\delta}) = \hat{\mathcal{K}} \cdot f_\theta(x_l)$ . Thus, the loss function can be expressed as:

$$\mathcal{L}_{dynamic} = \mathcal{L}_{MSE}(f_\theta(X_{back}), \hat{\mathcal{K}} \cdot f_\theta(X_{fore})), \quad (6)$$

where  $\mathcal{L}_{MSE}$  is the Mean Square Error loss. Minimizing this loss ensures that for every video clip, given the representation of the first frame, the trajectories of the frame representations can be accurately modeled by a linear operator  $\hat{\mathcal{K}}$ . Therefore, we explicitly model the dynamic semantics to  $f_\theta$  with the Dynamic Module.

Note that the ability of the dynamic module to extract dynamic semantics is predicated on the premise that the feature extractor can first extract static semantics. That is, the learning process can be seen as a decoupling process, where the feature extractor learns static semantics first, followed by dynamic semantics, with the learning processes of the two being independent and not interfering with each other. In Subsection 3.3, we obtain that during the learning of dynamic semantics, static semantics can become confounded. This is because the feature extractor does not distinguish between types of semantics but instead learns all semantics simultaneously. Also, according to [27, 43], we can obtain that learning representations by uncoupling allows learning real causal relations and is not affected by semantic confounding. Therefore, the dynamic module does not face the issue of static semantic confusion.

## 4.2 Stratify Module

In the previous subsection, we propose to obtain  $\hat{\mathcal{K}}$  through dynamic module learning. Ideally, the obtained  $\mathcal{K}$  should encompass all the dynamic semantics of the video segment  $X$ .

In video clips, the trends for different objects vary. For instance, the physical objects in the video part often remain unchanged, while the characters in the video move rapidly. However, given a representation of a video clip, it is difficult to directly ascertain which part of the video frame is the physical object and which part consists of moving characters.

Note that when transforming Equation (3) into Equation (4), we can perform eigenvalue decomposition on the  $\mathcal{K}$ , which is expressed as  $\mathcal{K} = \Phi \Lambda \Phi^{-1}$ , where  $\Phi = [\varphi_1, \dots, \varphi_M] \in \mathbb{C}^{M \times M}$  are eigenvectors,  $\Lambda$  is the eigenvalue matrix, where  $\Lambda = \text{diag}([\lambda_1, \dots, \lambda_M]) \in \mathbb{C}^{M \times M}$ ,  $\text{diag}$  means that the eigenvalues are in the form of a diagonal matrix. Also, they satisfy:

$$\mathcal{K}\Phi = \Phi\Lambda. \quad (7)$$

Then, according to Equation (5), we have:

$$\begin{aligned} \mathcal{G}(x_{t+1}) &= \mathcal{K}\mathcal{G}(x_t), \\ \mathcal{G}(x_{t+1}) &= \Phi\Lambda\Phi^{-1}\mathcal{G}(x_t), \\ \mathcal{G}(x_{t+2}) &= \Phi\Lambda\Phi^{-1}\Phi\Lambda\Phi^{-1}\mathcal{G}(x_t), \\ &\vdots \\ \mathcal{G}(x_{t+k}) &= \Phi\Lambda^k\Phi^{-1}\mathcal{G}(x_t). \end{aligned} \quad (8)$$

We assume that Equation (8) is calculated in complex space. Let  $\mathbf{b} = \Phi^{-1}\mathcal{G}(x_t) = [b_1, \dots, b_M]^T \in \mathbb{C}^{M \times 1}$ , we can obtain that each element  $b_m$  of  $\mathbf{b}$  represents the projection of the original frame in the  $m$ -th direction  $\varphi_m$ . Then, we have for the  $t+k$ -th frame,  $\Phi^{-1}\mathcal{G}(x_{t+k}) = \Lambda^k \mathbf{b}$ .

We define the  $m$ -th element in  $\Lambda$  as  $\lambda_m$ . Because that  $\lambda_m \in \mathbb{C}$  is a complex number, we can reformulate  $\lambda_m$  as  $\lambda_m = \text{Re}_m + j\text{Im}_m$ . It consists of a real part  $\text{Re}_m$  and an imaginary part  $\text{Im}_m$ , and  $j$  is the imaginary unit. Also, we can obtain that  $\lambda_m = |\lambda_m|e^{j\text{Arg}(\lambda_m)}$ , where  $|\lambda_m| = \sqrt{\text{Re}_m^2 + \text{Im}_m^2}$  is the magnitude of  $\lambda_m$ ,  $\text{Arg}(\lambda_m) = \text{atan2}(\text{Re}_m, \text{Im}_m)$  is the argument of  $\lambda_m$ ,  $\text{atan2}$  is the 2-argument arctangent function. According to Euler's formula, we have:

$$\begin{aligned} \lambda_m^k &= |\lambda_m|^k e^{j\text{Arg}(\lambda_m)k}, \\ &= |\lambda_m|^k (\cos(\text{Arg}(\lambda_m)k) + j \sin(\text{Arg}(\lambda_m)k)). \end{aligned} \quad (9)$$

Based on Equation (9), we can infer that if  $\varphi_m$  is related to the dynamic semantic, we have that the magnitude of  $|\lambda_m|$  determines how fast the frame can change in the direction of  $\varphi_m$ , while  $\text{Arg}(\lambda_m)$  determines the oscillation of frames in the direction of  $\varphi_m$ . Meanwhile, when  $|\lambda_m| \approx 1$  and  $\text{Arg}(\lambda_m) \approx 0$ , the projection in direction  $\varphi_m$  merely changes over time. In this condition, we can regard  $\varphi_m$  as related to the static semantic. In all, from the above discussion, we can obtain that the element value  $|\lambda_m|$  in  $\Lambda$  can determine whether  $\varphi_m$  is related to static semantic or dynamic semantic. Therefore, we propose that when  $|\lambda_m| \geq \varsigma$  and  $\text{Arg}(\lambda_m) \leq \omega$ , we regard  $\varphi_m$  as related to static semantic, otherwise, we regard  $\varphi_m$  as related to dynamic semantic.

### 4.3 Static Module

In this subsection, we introduce the proposed static module, which aims to empower the feature extractor obtained from v-CL to precisely mine static semantics in video samples.

From Subsection 3.3, a problem is that dynamic semantics can confound the learning of static semantics. To solve this, we propose to utilize backdoor adjustment [43] to eliminate the effect of dynamic semantics while learning static semantics. In Subsection 3.2, the feature extractor obtained directly via v-CL is mainly concerned with the extraction of static semantics. This provides us with ideas on how to utilize backdoor adjustment, i.e., incorporate backdoor adjustment directly into the training process of v-CL, so that v-CL focuses all on static semantics and ignores dynamic semantics when learning the feature extractor. Since v-CL is modeled based on the similarity between samples, e.g., positive samples should be as similar as possible to each other in the feature space. From there, it follows that for v-CL to learn static features better, the similarity between samples in the feature space should be determined by the static semantically relevant feature representations only. This gives us ideas on where to make backdoor adjustments, i.e., modulating the similarity metric between samples.

Based on the above discussion, we propose the backdoor adjustment guided similarity metric. Since we need to compute the similarity between all other samples and the anchor, given a sample  $X_i^p$ , we rewrite the similarity  $\text{sim}(X_i^p, X^+)$  as  $P(X^+|X_i^p)$ , and the more similar  $X_i^p$  and  $X^+$  are, the larger  $P(X^+|X_i^p)$  is. Then, based on the definition of backdoor adjustment in causal inference [43], we can eliminate the confounding influence of dynamic semantics in the following form:

$$P(X^+|do(X_i^p)) = \sum_j P(X^+|X_i^p, \varphi_j)P(\varphi_j), \quad (10)$$

where  $P(X^+|do(X_i^p))$  denotes the similarity measure after backdoor adjustment,  $do$  is the adjustment flag, and  $\varphi_j$  represents the  $j$ -th dynamic semantic vector obtained in advance. We can obtain dynamic semantics based on the proposed stratify module.

During the training phase, all calculations are done in the latent feature space, thus, we implement  $P(X^+|X_i^p, \varphi_j)$  as:

$$P(X^+|X_i^p, \varphi_j) = -\log \frac{\exp(|Z_i^p \cdot \varphi_j - Z^+ \cdot \varphi_j|/\alpha)}{\sum_{t=1, Z_t^p \neq Z^+}^{t=2\varrho N} \exp(|Z_t^p \cdot \varphi_j - Z^+ \cdot \varphi_j|/\alpha)} \quad (11)$$

where  $Z^+$  is the representation of  $X^+$ ,  $Z_i^p$  is the representation of  $X_i^p$ , and  $\alpha$  is a pre-given hyperparameter. Assuming that we are given  $J$  dynamic semantics in advance, then  $P(\varphi_j)$  can be implemented as  $1/J$ . Finally, to allow the feature extractor to accurately mine static semantics without being confounded by dynamic semantics, we constrain  $\text{sim}(X_i^p, X^+) = P(X^+|do(X_i^p))$  in v-CL.

### 4.4 Overall Objective

To learn static and dynamic features in a decoupled manner, we propose a bi-level optimization objective, expressed as:

$$\begin{aligned} \min_{\theta} \mathcal{L}_{cl}(f_{\theta}^*) + \nu \mathcal{L}_{dynamic}(f_{\theta}^*) \quad (12) \\ \text{s.t. } f_{\theta}^* = \arg \min_{f_{\theta}} \mathcal{L}_{ct}(f_{\theta}, do) \end{aligned}$$

where  $\nu$  is a hyperparameter and  $\mathcal{L}_{ct}(f_{\theta}, do)$  denotes that  $\mathcal{L}_{ct}(f_{\theta})$  is calculated based on the backdoor adjustment guided similarity metric proposed in Static module. The  $\mathcal{L}_{cl}(f_{\theta}^*)$  and  $\mathcal{L}_{dynamic}(f_{\theta}^*)$  represent that  $\mathcal{L}_{cl}$  and  $\mathcal{L}_{dynamic}$  are calculated based on  $f_{\theta}^*$ . This process consists of two stages. In the first stage, we have:

$$f_{\theta}^* \leftarrow f_{\theta} - \gamma \nabla_{f_{\theta}} \mathcal{L}_{ct}(f_{\theta}, do) \quad (13)$$

where  $\gamma$  is the learning rate. This stage corresponds to the proposed static module. Thus,  $f_{\theta}^*$  can only extract static semantic. In the second stage, we have:

$$f_{\theta} \leftarrow f_{\theta} - \gamma \nabla_{f_{\theta}} [\mathcal{L}_{cl}(f_{\theta}^*) + \nu \mathcal{L}_{dynamic}(f_{\theta}^*)] \quad (14)$$

Because  $f_{\theta}^*$  can only extract static semantics, so  $f_{\theta}^*$  satisfies the constraints on  $f_{\theta}$  in dynamic module. Thus, we can obtain that  $\mathcal{L}_{dynamic}(f_{\theta}^*)$  corresponds to the dynamic module, and learning with  $\mathcal{L}_{dynamic}(f_{\theta}^*)$  can be such that the learned feature extractor extracts only dynamic semantics. From Subsection 3.2, we can obtain that learning with  $\mathcal{L}_{cl}$  can extract both static and dynamic semantics at the same time, which can be viewed as a fusion learning process of static and dynamic semantics. In all, the  $f_{\theta}^*$  in the term  $\mathcal{L}_{cl}(f_{\theta}^*)$  is to constrain v-CL to learn static semantics, the term  $\mathcal{L}_{dynamic}(f_{\theta}^*)$  is to constrain v-CL to learn dynamic semantics, the term  $\mathcal{L}_{cl}(f_{\theta}^*)$  is to constrain v-CL to incorporate both the learned static and dynamic semantics into a single feature representation. **Note that all notations used in this paper and their specific meanings are displayed in tabular form in the Appendix.**

## 5 EXPERIMENTS

### 5.1 Experimental Setup

**Datasets.** We use five action recognition datasets: Kinetics400 [31], UCF101 [52], HMDB51 [35], Something-Something v2 [21](SSv2) and FineGym [51] (Gym99). Specifically, Kinetics400 is a large-scale dataset with 24K realistic action videos from 400 action categories, which is one of the largest and most widely used datasets for video pre-trained models. UCF101 and HMDB51 are two standard datasets for evaluating the performance of action recognition. SSv2 and FineGym are two motion-aware datasets that encompass a wider variety of action labels. We also provide experimental results of action detection on the AVA dataset [23] in the Appendix.

**Networks.** We implement the feature extractor  $f_{\theta}$  with Slow-R50 [13] by default. We also integrate BOLD-DI with the best performance v-CL method, v-BYOL on other networks, namely S3D-G

**Table 1: Finetuning Results (average of 3 splits) for action classification on UCF101 and HMDB51. Self-supervised pretraining is done on Kinetics 400 datasets. All results without special notations are from the original article. Results with † are reproduced according to the open-source repositories. As for modality, "V" indicates RGB video, "A" indicates audio, and "F" indicates optical flow.  $\varrho$  is the number of positive samples. Results using R(2+1)D-18 and S3D-G are in the Appendix.**

Method	Resolution	Frames	Architecture	Param.	Epochs	Modality	UCF101	HMDB51
VTHCL [67]	224×224	8	R3D-18	13.5M	200	V	80.6	48.6
TCLR [10]	112×112	16	R3D-18	13.5M	100	V	85.4	55.4
VideoMoCo [41]	112×112	16	R3D-18	13.5M	200	V	74.1	43.6
SLIC [32]	128×128	32	R3D-18	13.5M	150	V	83.2	52.2
MACLR [65]	112×112	32	R3D-18	13.5M	600	V	91.3	62.1
v-BYOL <sup>†</sup> <sub><math>\varrho=4</math></sub>	112×112	16	R3D-18	13.5M	200	V	88.3	69.3
v-BYOL <sub><math>\varrho=4</math></sub> + BOLD-DI	112×112	16	R3D-18	13.5M	200	V	<b>92.3 († 3.5)</b>	<b>71.1 († 1.8)</b>
CVRL [44]	224×224	32	R3D-50	31.8M	800	V	92.2	66.7
MACLR [65]	224×224	32	R3D-50	31.8M	600	V	94.0	67.4
MACLR [65]	224×224	32	R3D-50	31.8M	600	V + F	94.2	67.2
v-SimCLR <sub><math>\varrho=2</math></sub> [14]	224×224	8	R3D-50	31.8M	200	V	88.9	67.2 <sup>†</sup>
v-SwAV <sub><math>\varrho=2</math></sub> [14]	224×224	8	R3D-50	31.8M	200	V	87.3	68.3 <sup>†</sup>
v-MoCo <sub><math>\varrho=4</math></sub> [14]	224×224	8	R3D-50	31.8M	200	V	93.5	71.6 <sup>†</sup>
v-BYOL <sub><math>\varrho=4</math></sub> [14]	224×224	8	R3D-50	31.8M	200	V	94.2	72.1
v-BYOL <sub><math>\varrho=4</math></sub> [14]	224×224	16	R3D-50	31.8M	200	V	95.5	73.6
v-SimCLR <sub><math>\varrho=2</math></sub> + BOLD-DI	224×224	8	R3D-50	31.8M	200	V	90.2 († 1.3)	70.6 († 3.4)
v-SwAV <sub><math>\varrho=2</math></sub> + BOLD-DI	224×224	8	R3D-50	31.8M	200	V	92.2 († 4.9)	73.3 († 5.0)
v-MoCo <sub><math>\varrho=4</math></sub> + BOLD-DI	224×224	8	R3D-50	31.8M	200	V	94.4 († 0.9)	75.2 († 3.6)
v-BYOL <sub><math>\varrho=4</math></sub> + BOLD-DI	224×224	8	R3D-50	31.8M	200	V	95.1 († 0.9)	74.6 († 2.5)
v-BYOL <sub><math>\varrho=4</math></sub> + BOLD-DI	224×224	16	R3D-50	31.8M	200	V	<b>96.5 († 1.0)</b>	<b>75.8 († 2.2)</b>
VideoMAE [58]	224×224	16	ViT-B	87M	800	V	96.1	73.3
MotionMAE [68]	224×224	16	ViT-B	87M	800	V	96.1	73.3
MME [53]	224×224	16	ViT-B	87M	800	V	96.5	78.0
MGM [12]	224×224	16	ViT-B	87M	800	V	91.9	69.7
v-BYOL <sup>†</sup> <sub><math>\varrho=4</math></sub>	224×224	16	ViT-B	87M	800	V	95.2	76.8
v-BYOL <sub><math>\varrho=4</math></sub> + BOLD-DI	224×224	16	ViT-B	87M	800	V	<b>96.9 († 1.7)</b>	<b>78.2 († 1.4)</b>

**Table 2: The top-1 accuracy (%) of action classification on motion-aware datasets Something-Something v2 and FineGym. The results are either from SEVERE [55] or the original paper. The results with † are reproduced with open-source repositories.  $\varrho$  is the number of positive samples.**

Method	backbone	SSv2	Gym99
GDT [42]	R(2+1)D-18	58.0	90.5
TCLR [10]	R(2+1)D-18	59.8	91.6
TubeCo [56]	R(2+1)D-18	60.2	92.8
VideoMoCo [41]	R(2+1)D-18	59.0	90.3
v-BYOL <sup>†</sup> <sub><math>\varrho=4</math></sub>	R(2+1)D-18	56.7	88.6
v-BYOL <sub><math>\varrho=4</math></sub> + BOLD-DI	R(2+1)D-18	<b>61.7 († 5.0)</b>	<b>93.0 († 4.4)</b>
SVT [47]	ViT-B	59.2	62.3
v-BYOL <sup>†</sup> <sub><math>\varrho=4</math></sub>	ViT-B	58.7	61.4
v-BYOL <sub><math>\varrho=4</math></sub> + BOLD-DI	ViT-B	<b>64.4 († 5.7)</b>	<b>64.8 († 3.4)</b>

[66], R3D-18[29], R(2+1)D-18 [59], and ViT-B [5], for a fair comparison with prior works. Full results are provided in the Appendix.

**Pretraining Setting.** We follow the pretraining procedure in [14] and pre-train the backbone networks on the Kinetics 400 [31] dataset. We integrate our method with 4 video contrastive learning

methods, namely v-MoCo, v-BYOL, v-SimCLR, and v-SwAV. The projection MLP output dimensions are 128 for v-MoCo, v-SimCLR, v-SwAV, and 256 for v-BYOL following original methods[7, 8, 22, 26]. The default epoch for pre-training is set to 200, and the total training hours for v-SimCLR + BOLD-DI, v-BYOL + BOLD-DI, v-MoCo + BOLD-DI, v-SwAV + BOLD-DI are 24.6, 30.8, 22.5, 27.2 hours respectively on 16 NVIDIA V100 GPUs. The projection head  $f_{\epsilon}$  for v-MoCo, v-SimCLR, and v-SwAV is a 3-layer MLP with a hidden dimension of 2048. The projection and prediction MLPs for v-BYOL have 2 layers with hidden dimension 4096. The temperature parameter  $\alpha = 0.1$  for v-SimCLR, v-MoCo and v-SwAV. We apply SGD with LARS [70] as the optimizer. The synchronized batch normalization is used for all methods except v-MoCo.

## 5.2 Action Recognition

**Evaluation Protocols.** After pre-training, in accordance with the standard evaluation protocols [10, 14, 44, 55], we perform a supervised fine-tuning of the feature extractor on downstream datasets. During this process, the entire set of weights for the feature extractor is trained with supervision, complemented by an additional classification layer. The results of UCF101 and HMDB51 are presented in Table 1. To ensure a fair comparison, we evaluate our

**Table 3: Linear evaluation results on the Kinetics-400 dataset, where  $\rho$ ,  $L$ , and  $\delta$  denote the number of positive samples, clip length, and stride, respectively.**

Method	$\rho$	$L$	$\delta$	Top-1 Acc. (%)
supervised	-	8	8	74.7
v-SimCLR [14]	2	8	8	60.5
v-BYOL [14]	2	8	8	65.8
v-MoCo [14]	2	8	8	65.8
v-SwAV [14]	2	8	8	61.6
v-SimCLR + BOLD-DI	2	8	8	63.7 ( $\uparrow$ 3.2)
v-BYOL + BOLD-DI	2	8	8	67.8 ( $\uparrow$ 2.0)
v-MoCo + BOLD-DI	2	8	8	<b>68.5</b> ( $\uparrow$ 2.7)
v-SwAV + BOLD-DI	2	8	8	64.4 ( $\uparrow$ 2.8)
v-MoCo [14]	4	8	8	67.8
v-BYOL [14]	4	8	8	68.9
v-MoCo [14]	2	16	4	67.6
v-BYOL [14]	4	16	4	71.5
v-MoCo + BOLD-DI	4	8	8	70.4 ( $\uparrow$ 2.6)
v-BYOL + BOLD-DI	4	8	8	71.6 ( $\uparrow$ 2.7)
v-MoCo + BOLD-DI	2	16	4	69.3 ( $\uparrow$ 1.7)
v-BYOL + BOLD-DI	4	16	4	<b>73.8</b> ( $\uparrow$ 2.3)

method on commonly utilized networks and provide details regarding the input resolution and the number of frames used. The results of Something-Something v2 and FineGym are presented in Table 2, and follow the same setup as in the SEVERE benchmark [55]. We then provide linear evaluation results on the Kinetics-400 dataset, where the weights of the feature extractor are frozen, and an additional linear classification layer is trained on top. The results with different positive samples, clip length, and stride are presented in Table 3. During inference, we uniformly sample three clips from a video and average the softmax scores for the prediction.

**Results.** From Table 1, we can observe that under the same number of epochs and the same resolution and frame length, our proposed BOLD-DI consistently improves the accuracies of the v-CL methods and outperforms the prior works under the same experimental setting. Our methods improved the performance of v-CL methods on UCF101 with an average increase of 2.1% and an average improvement of 2.7% on HMDB51. From Table 2, we can observe that the original v-BYOL performs poorly compared to prior works, while v-BYOL + BOLD-DI significantly improves the performance of v-BYOL on both SSv2 and Gym99. Specifically, when using ViT-B, the v-BYOL + BOLD-DI improved the performance of v-BYOL in SSv2 by 5.6%. This demonstrates the effectiveness of our proposed method when learning dynamic semantics. From Table 3, we can observe that under different setting, our proposed v-CL + BOLD-DI consistently improves the performance of the corresponding v-CL method by an average of 2.5%.

### 5.3 Ablation Studies

In this section, we conduct ablation experiments from the following aspects: (1) The performance under different pretraining epochs. (2) The impact of bi-level optimization. Additional ablation experiments include (1) The impact of different choices of bi-level

**Table 4: Linear evaluation on Kinetics 400 with different pre-training epochs. For all results, the number of positive samples  $\rho = 2$  and frame length  $L = 8$ , stride  $\delta = 8$ .**

Epochs	50	100	200	400	800
v-SimCLR	45.7	57.3	60.5	62.0	61.8
v-BYOL	30.2	47.6	65.8	66.9	66.2
v-MoCo	52.6	60.5	65.8	67.4	67.4
v-SwAV	55.9	59.4	61.6	62.9	63.2
v-SimCLR + BOLD-DI	52.7	60.4	63.7	63.8	64.2
v-BYOL + BOLD-DI	44.6	52.8	67.8	67.9	67.8
v-MoCo + BOLD-DI	55.9	63.4	68.5	68.8	68.9
v-SwAV + BOLD-DI	58.4	62.3	64.4	64.8	65.1

**Table 5: Linear evaluation on Kinetics400 without using bi-level optimization. The results with \* denotes minimizing the  $\mathcal{L}_{cl}$ ,  $\mathcal{L}_{dynamic}$  and  $\mathcal{L}_{backdoor}$  simultaneously. The pre-training epoch is 200, with  $\rho = 2$ ,  $L = 8$ ,  $\delta = 8$ .**

Method	v-SimCLR*	v-BYOL*	v-MoCo*	v-SwAV*
Top-1 Acc. (%)	61.4	66.7	66.2	63.5

optimization implementation, (2) The impact of different numbers of eigenvectors  $M$ , (3) Additional results on Experiment 2 from Subsection 3.2, (4) The influence of hyperparameters, and (5) The effect of only using  $\mathcal{L}_{dynamic}$  are illustrated in the Appendix.

**Ablation on pre-training epochs.** We conduct an ablation study on the impact of longer pre-training epochs in Table 4, comparing the linear evaluation performance on the Kinetics-400 dataset. From Table 4, we can observe that as the number of pre-training epochs increases, the performance of v-CL + BOLD-DI consistently outperforms v-CL. While a longer training duration generally leads to improved performance, the results for 800 epochs show no significant gain over those for 200 epochs ( $< 1\%$ ). Moreover, our proposed v-CL + BOLD-DI converges faster than the standard v-CL methods, demonstrating the effectiveness of our proposed method.

**Ablation on Bi-level Optimization.** We also conduct an ablation study by replacing the bi-level optimization problem in Equation (12) with a single-level optimization problem. Where  $\mathcal{L}_{cl}(f_{\theta}^*)$ ,  $\mathcal{L}_{dynamic}(f_{\theta}^*)$  and  $\mathcal{L}_{cl}((f_{\theta}, do))$  are minimized simultaneously. The results of linear evaluation on Kinetics400 are demonstrated in Table 5, where we denote the results with \*. By comparing the results in Table 5 with those in Table 3, we can observe that the results of v-CL\* still outperform the corresponding v-CL methods, but are lower than the results achieved by v-CL + BOLD-DI. This phenomenon underscores the necessity of bi-level optimization and reveals the correctness of our analysis, as discussed in Section 4.4.

## 6 CONCLUSION

In this work, we discover through experiments that v-CL methods learn primary static rather than dynamic semantics. Guided by thorough analysis, we propose *Bi-level Optimization of Learning Dynamic with Decoupling and Intervention* (BOLD-DI) to learn both static and dynamic semantics in a decoupled way. Our method can seamlessly integrate with existing v-CL approaches, demonstrating



its effectiveness in capturing both static and dynamic semantics. Empirical results underscore the effectiveness of our method.

## REFERENCES

- [1] Adrien Bardes, Jean Ponce, and Yann LeCun. 2022. VICReg: Variance-Invariance-Covariance Regularization for Self-Supervised Learning. <https://doi.org/10.48550/arXiv.2105.04906> arXiv:2105.04906 [cs].
- [2] Sagie Benaim, Ariel Ephrat, Oran Lang, Inbar Mosseri, William T Freeman, Michael Rubinstein, Michal Irani, and Tali Dekel. 2020. Speednet: Learning the speediness in videos. In *Proceedings of the IEEE/CVF Conference on Computer Vision and Pattern Recognition*. 9922–9931.
- [3] Yoshua Bengio, Aaron Courville, and Pascal Vincent. 2014. Representation Learning: A Review and New Perspectives. <https://doi.org/10.48550/arXiv.1206.5538> [cs].
- [4] Nimrod Berman, Ilan Naiman, and Omri Azencot. 2022. Multifactor Sequential Disentanglement via Structured Koopman Autoencoders. In *The Eleventh International Conference on Learning Representations*.
- [5] Gedas Bertasius, Heng Wang, and Lorenzo Torresani. 2021. Is space-time attention all you need for video understanding?. In *ICML*, Vol. 2. 4.
- [6] Bingni W Brunton, Lise A Johnson, Jeffrey G Ojemann, and J Nathan Kutz. 2016. Extracting spatial–temporal coherent patterns in large-scale neural recordings using dynamic mode decomposition. *Journal of neuroscience methods* 258 (2016), 1–15.
- [7] Mathilde Caron, Ishan Misra, Julien Mairal, Priya Goyal, Piotr Bojanowski, and Armand Joulin. 2021. Unsupervised Learning of Visual Features by Contrasting Cluster Assignments. <https://doi.org/10.48550/arXiv.2006.09882> arXiv:2006.09882 [cs].
- [8] Ting Chen, Simon Kornblith, Mohammad Norouzi, and Geoffrey Hinton. 2020. A Simple Framework for Contrastive Learning of Visual Representations. In *Proceedings of the 37th International Conference on Machine Learning*. PMLR, 1597–1607. <https://proceedings.mlr.press/v119/chen20j.html> ISSN: 2640-3498.
- [9] Sang Keun Choe, Willie Neiswanger, Pengtao Xie, and Eric Xing. 2022. Betty: An Automatic Differentiation Library for Multilevel Optimization. [https://openreview.net/forum?id=LV\\_MeMS38Q9](https://openreview.net/forum?id=LV_MeMS38Q9)
- [10] Ishan Dave, Rohit Gupta, Mamshad Nayeem Rizve, and Mubarak Shah. 2022. TCLR: Temporal Contrastive Learning for Video Representation. *Computer Vision and Image Understanding* 219 (June 2022), 103406. <https://doi.org/10.1016/j.cviu.2022.103406> arXiv:2101.07974 [cs].
- [11] N. Benjamin Erichson, Steven L. Brunton, and J. Nathan Kutz. 2019. Compressed Dynamic Mode Decomposition for Background Modeling. *Journal of Real-Time Image Processing* 16, 5 (Oct. 2019), 1479–1492. <https://doi.org/10.1007/s11554-016-0655-2> arXiv:1512.04205 [cs].
- [12] David Fan, Jue Wang, Shuai Liao, Yi Zhu, Vimal Bhat, Hector Santos-Villalobos, Rohith MV, and Xinyu Li. 2023. Motion-guided masking for spatiotemporal representation learning. In *Proceedings of the IEEE/CVF International Conference on Computer Vision*. 5619–5629.
- [13] Christoph Feichtenhofer, Haoqi Fan, Jitendra Malik, and Kaiming He. 2019. Slow-Fast Networks for Video Recognition. <https://doi.org/10.48550/arXiv.1812.03982> arXiv:1812.03982 [cs].
- [14] Christoph Feichtenhofer, Haoqi Fan, Bo Xiong, Ross Girshick, and Kaiming He. 2021. A Large-Scale Study on Unsupervised Spatiotemporal Representation Learning. <https://doi.org/10.48550/arXiv.2104.14558> arXiv:2104.14558 [cs].
- [15] Christoph Feichtenhofer, Yanghao Li, and Kaiming He. 2022. Masked autoencoders as spatiotemporal learners. *Advances in neural information processing systems* 35 (2022), 35946–35958.
- [16] Basura Fernando, Hakan Bilen, Efstratios Gavves, and Stephen Gould. 2017. Self-supervised video representation learning with odd-one-out networks. In *Proceedings of the IEEE conference on computer vision and pattern recognition*. 3636–3645.
- [17] Chelsea Finn, Pieter Abbeel, and Sergey Levine. 2017. Model-agnostic meta-learning for fast adaptation of deep networks. In *International conference on machine learning*. PMLR, 1126–1135.
- [18] Ross Girshick. 2015. Fast r-cnn. In *Proceedings of the IEEE international conference on computer vision*. 1440–1448.
- [19] Ross Girshick, Ilija Radosavovic, Georgia Gkioxari, Piotr Dollár, and Kaiming He. 2018. Detectron. <https://github.com/facebookresearch/detectron>.
- [20] Madelyn Glymour, Judea Pearl, and Nicholas P. Jewell. 2016. *Causal Inference in Statistics: A Primer*. John Wiley & Sons. Google-Books-ID: 10V2CwAAQBAJ.
- [21] Raghav Goyal, Samira Ebrahimi Kahou, Vincent Michalski, Joanna Materzynska, Susanne Westphal, Heuna Kim, Valentin Haenel, Ingo Freund, Peter Yianilos, Moritz Mueller-Freitag, et al. 2017. The "something something" video database for learning and evaluating visual common sense. In *Proceedings of the IEEE international conference on computer vision*. 5842–5850.
- [22] Jean-Bastien Grill, Florian Strub, Florent Altché, Corentin Tallec, Pierre Richemond, Elena Buchatskaya, Carl Doersch, Bernardo Avila Pires, Zhaohan Guo, Mohammad Gheshlaghi Azar, Bilal Piot, koray kavukcuoglu, Remi Munos, and Michal Valko. 2020. Bootstrap Your Own Latent - A New Approach to Self-Supervised Learning. In *Advances in Neural Information Processing Systems*, Vol. 33. Curran Associates, Inc., 21271–21284. <https://proceedings.neurips.cc/paper/2020/hash/f3ada80d5c4ee70142b17b8192b2958e-Abstract.html>
- [23] Chunhui Gu, Chen Sun, David A Ross, Carl Vondrick, Caroline Pantofaru, Yeqing Li, Sudheendra Vijayanarasimhan, George Toderici, Susanna Ricco, Rahul Sukthankar, et al. 2018. Ava: A video dataset of spatio-temporally localized atomic visual actions. In *Proceedings of the IEEE conference on computer vision and pattern recognition*. 6047–6056.
- [24] Tengda Han, Weidi Xie, and Andrew Zisserman. 2021. Self-supervised Co-training for Video Representation Learning. <https://doi.org/10.48550/arXiv.2010.09709> arXiv:2010.09709 [cs].
- [25] Kaiming He, Xinlei Chen, Saining Xie, Yanghao Li, Piotr Dollár, and Ross Girshick. 2022. Masked autoencoders are scalable vision learners. In *Proceedings of the IEEE/CVF conference on computer vision and pattern recognition*. 16000–16009.
- [26] Kaiming He, Haoqi Fan, Yuxin Wu, Saining Xie, and Ross Girshick. 2020. Momentum Contrast for Unsupervised Visual Representation Learning. 9729–9738. [https://openaccess.thecvf.com/content\\_CVPR\\_2020/html/He\\_Momentum\\_Contrast\\_for\\_Unsupervised\\_Visual\\_Representation\\_Learning\\_CVPR\\_2020\\_paper.html](https://openaccess.thecvf.com/content_CVPR_2020/html/He_Momentum_Contrast_for_Unsupervised_Visual_Representation_Learning_CVPR_2020_paper.html)
- [27] Ziniu Hu, Zhe Zhao, Xinyang Yi, Tiansheng Yao, Lichan Hong, Yizhou Sun, and Ed Chi. 2022. Improving multi-task generalization via regularizing spurious correlation. *Advances in Neural Information Processing Systems* 35 (2022), 11450–11466.
- [28] Simon Jenni, Givi Meishvili, and Paolo Favaro. 2020. Video Representation Learning by Recognizing Temporal Transformations. <https://doi.org/10.48550/arXiv.2007.10730> arXiv:2007.10730 [cs].
- [29] Shuiwang Ji, Wei Xu, Ming Yang, and Kai Yu. 2012. 3D convolutional neural networks for human action recognition. *IEEE transactions on pattern analysis and machine intelligence* 35, 1 (2012), 221–231.
- [30] Longlong Jing and Yingli Tian. 2021. Self-Supervised Visual Feature Learning With Deep Neural Networks: A Survey. *IEEE Transactions on Pattern Analysis and Machine Intelligence* 43, 11 (2021), 4037–4058. <https://doi.org/10.1109/TPAMI.2020.2992393> Conference Name: IEEE Transactions on Pattern Analysis and Machine Intelligence.
- [31] Will Kay, Joao Carreira, Karen Simonyan, Brian Zhang, Chloe Hillier, Sudheendra Vijayanarasimhan, Fabio Viola, Tim Green, Trevor Back, Paul Natsev, et al. 2017. The kinetics human action video dataset. *arXiv preprint arXiv:1705.06950* (2017).
- [32] Salar Hosseini Khorasgani, Yuxuan Chen, and Florian Shkurti. 2022. SLIC: Self-Supervised Learning with Iterative Clustering for Human Action Videos. <http://arxiv.org/abs/2206.12534> arXiv:2206.12534 [cs].
- [33] Bernard O Koopman. 1931. Hamiltonian systems and transformation in Hilbert space. *Proceedings of the National Academy of Sciences* 17, 5 (1931), 315–318.
- [34] Haofei Kuang, Yi Zhu, Zhi Zhang, Xinyu Li, Joseph Tighe, Sören Schwertfeger, Cyrill Stachniss, and Mu Li. 2021. Video contrastive learning with global context. In *Proceedings of the IEEE/CVF International Conference on Computer Vision*. 3195–3204.
- [35] Hildegard Kuehne, Hueihan Jhuang, Estíbaliz Garrote, Tomaso Poggio, and Thomas Serre. 2011. HMDB: a large video database for human motion recognition. In *2011 International conference on computer vision*. IEEE, 2556–2563.
- [36] Hanxiao Liu, Karen Simonyan, and Yiming Yang. 2018. Darts: Differentiable architecture search. *arXiv preprint arXiv:1806.09055* (2018).
- [37] Jonathan Lorraine, Paul Vicol, and David Duvenaud. 2020. Optimizing Millions of Hyperparameters by Implicit Differentiation. In *Proceedings of the Twenty Third International Conference on Artificial Intelligence and Statistics*. PMLR, 1540–1552. <https://proceedings.mlr.press/v108/lorraine20a.html> ISSN: 2640-3498.
- [38] David G Luenberger. 1979. *Dynamic Systems*. J. Wiley Sons.
- [39] Bethany Lusch, J Nathan Kutz, and Steven L Brunton. 2018. Deep learning for universal linear embeddings of nonlinear dynamics. *Nature communications* 9, 1 (2018), 4950.
- [40] Aaron van den Oord, Yazhe Li, and Oriol Vinyals. 2019. Representation Learning with Contrastive Predictive Coding. <https://doi.org/10.48550/arXiv.1807.03748> arXiv:1807.03748 [cs, stat].
- [41] Tian Pan, Yibing Song, Tianyu Yang, Wenhao Jiang, and Wei Liu. 2021. Videomoco: Contrastive video representation learning with temporally adversarial examples. In *Proceedings of the IEEE/CVF conference on computer vision and pattern recognition*. 11205–11214.
- [42] Mandela Patrick, Yuki Asano, Polina Kuznetsova, Ruth Fong, Joao F Henriques, Geoffrey Zweig, and Andrea Vedaldi. 2020. Multi-modal self-supervision from generalized data transformations. (2020).
- [43] Judea Pearl. 2009. *Causality*. Cambridge university press.
- [44] Rui Qian, Tianjian Meng, Boqing Gong, Ming-Hsuan Yang, Huisheng Wang, Serge Belongie, and Yin Cui. 2021. Spatiotemporal contrastive video representation learning. In *Proceedings of the IEEE/CVF Conference on Computer Vision and Pattern Recognition*. 6964–6974.
- [45] Aravind Rajeswaran, Chelsea Finn, Sham M. Kakade, and Sergey Levine. 2019. Meta-learning with implicit gradients. *Advances in neural information processing systems* 32 (2019). [https://proceedings.neurips.cc/paper\\_files/paper/2019/hash/072b030ba126b2f4b2374f342be9ed44-Abstract.html](https://proceedings.neurips.cc/paper_files/paper/2019/hash/072b030ba126b2f4b2374f342be9ed44-Abstract.html)

- [46] Aravind Rajeswaran, Igor Mordatch, and Vikash Kumar. 2020. A game theoretic framework for model based reinforcement learning. In *International conference on machine learning*. PMLR, 7953–7963.
- [47] Kanchana Ranasinghe, Muzammal Naseer, Salman Khan, Fahad Shahbaz Khan, and Michael S. Ryoo. 2022. Self-supervised Video Transformer. In *2022 IEEE/CVF Conference on Computer Vision and Pattern Recognition (CVPR)*. IEEE, New Orleans, LA, USA, 2864–2874. <https://doi.org/10.1109/CVPR52688.2022.00289>
- [48] Shaoqing Ren, Kaiming He, Ross Girshick, and Jian Sun. 2015. Faster r-cnn: Towards real-time object detection with region proposal networks. *Advances in neural information processing systems* 28 (2015).
- [49] Madeline C. Schiappa, Yogesh S. Rawat, and Mubarak Shah. 2022. Self-supervised learning for videos: A survey. *Comput. Surveys* (2022). Publisher: ACM New York, NY.
- [50] Peter J Schmid. 2010. Dynamic mode decomposition of numerical and experimental data. *Journal of fluid mechanics* 656 (2010), 5–28.
- [51] Dian Shao, Yue Zhao, Bo Dai, and Dahua Lin. 2020. Finegym: A hierarchical video dataset for fine-grained action understanding. In *Proceedings of the IEEE/CVF conference on computer vision and pattern recognition*. 2616–2625.
- [52] Khurram Soomro, Amir Roshan Zamir, and Mubarak Shah. 2012. UCF101: A dataset of 101 human actions classes from videos in the wild. *arXiv preprint arXiv:1212.0402* (2012).
- [53] Xinyu Sun, Peihao Chen, Liangwei Chen, Changhao Li, Thomas H. Li, Mingkui Tan, and Chuang Gan. 2023. Masked Motion Encoding for Self-Supervised Video Representation Learning. In *2023 IEEE/CVF Conference on Computer Vision and Pattern Recognition (CVPR)*. IEEE, Vancouver, BC, Canada, 2235–2245. <https://doi.org/10.1109/CVPR52729.2023.00222>
- [54] Naoya Takeishi, Yoshinobu Kawahara, and Takehisa Yairi. 2017. Learning Koopman invariant subspaces for dynamic mode decomposition. *Advances in neural information processing systems* 30 (2017).
- [55] Fida Mohammad Thoker, Hazel Doughty, Piyush Bagad, and Cees G. M. Snoek. 2022. How Severe Is Benchmark-Sensitivity in Video Self-supervised Learning? In *Computer Vision – ECCV 2022*. Vol. 13694. Springer Nature Switzerland. [https://doi.org/10.1007/978-3-031-19830-4\\_36](https://doi.org/10.1007/978-3-031-19830-4_36) Series Title: Lecture Notes in Computer Science.
- [56] Fida Mohammad Thoker, Hazel Doughty, and Cees Snoek. 2023. Tubelet-Contrastive Self-Supervision for Video-Efficient Generalization. <http://arxiv.org/abs/2303.11003> arXiv:2303.11003 [cs].
- [57] Yonglong Tian, Chen Sun, Ben Poole, Dilip Krishnan, Cordelia Schmid, and Phillip Isola. 2020. What Makes for Good Views for Contrastive Learning?. In *Advances in Neural Information Processing Systems*, Vol. 33. Curran Associates, Inc., 6827–6839. [https://proceedings.neurips.cc/paper\\_files/paper/2020/hash/4c2e5eaa9152079b9e95845750bb9ab-Abstract.html](https://proceedings.neurips.cc/paper_files/paper/2020/hash/4c2e5eaa9152079b9e95845750bb9ab-Abstract.html)
- [58] Zhan Tong, Yibing Song, Jue Wang, and Limin Wang. 2022. VideoMAE: Masked Autoencoders are Data-Efficient Learners for Self-Supervised Video Pre-Training. <https://doi.org/10.48550/arXiv.2203.12602> arXiv:2203.12602 [cs].
- [59] Du Tran, Heng Wang, Lorenzo Torresani, Jamie Ray, Yann LeCun, and Manohar Paluri. 2018. A closer look at spatiotemporal convolutions for action recognition. In *Proceedings of the IEEE conference on Computer Vision and Pattern Recognition*. 6450–6459.
- [60] Julius Von Kügelgen, Yash Sharma, Luigi Gresele, Wieland Brendel, Bernhard Schölkopf, Michel Besserve, and Francesco Locatello. 2021. Self-supervised learning with data augmentations provably isolates content from style. *Advances in neural information processing systems* 34 (2021), 16451–16467.
- [61] Jinpeng Wang, Yuting Gao, Ke Li, Jianguo Hu, Xinyang Jiang, Xiaowei Guo, Rongrong Ji, and Xing Sun. 2020. Enhancing Unsupervised Video Representation Learning by Decoupling the Scene and the Motion. <http://arxiv.org/abs/2009.05757> arXiv:2009.05757 [cs].
- [62] Jiangliu Wang, Jianbo Jiao, Linchao Bao, Shengfeng He, Yunhui Liu, and Wei Liu. 2019. Self-supervised spatio-temporal representation learning for videos by predicting motion and appearance statistics. In *Proceedings of the IEEE/CVF Conference on Computer Vision and Pattern Recognition*. 4006–4015.
- [63] Jiangliu Wang, Jianbo Jiao, and Yun-Hui Liu. 2020. Self-supervised Video Representation Learning by Pace Prediction. <https://doi.org/10.48550/arXiv.2008.05861> arXiv:2008.05861 [cs].
- [64] Limin Wang, Bingkun Huang, Zhiyu Zhao, Zhan Tong, Yinan He, Yi Wang, Yali Wang, and Yu Qiao. 2023. Videomae v2: Scaling video masked autoencoders with dual masking. In *Proceedings of the IEEE/CVF Conference on Computer Vision and Pattern Recognition*. 14549–14560.
- [65] Fanyi Xiao, Joseph Tighe, and Davide Modolo. 2022. MaCLR: Motion-Aware Contrastive Learning of Representations for Videos. In *Computer Vision – ECCV 2022*, Shai Avidan, Gabriel Brostow, Moustapha Cissé, Giovanni Maria Farinella, and Tal Hassner (Eds.). Vol. 13695. Springer Nature Switzerland, Cham, 353–370. [https://doi.org/10.1007/978-3-031-19833-5\\_21](https://doi.org/10.1007/978-3-031-19833-5_21) Series Title: Lecture Notes in Computer Science.
- [66] Saining Xie, Chen Sun, Jonathan Huang, Zhuowen Tu, and Kevin Murphy. 2018. Rethinking spatiotemporal feature learning: Speed-accuracy trade-offs in video classification. In *Proceedings of the European conference on computer vision (ECCV)*. 305–321.
- [67] Ceyuan Yang, Yinghao Xu, Bo Dai, and Bolei Zhou. 2020. Video Representation Learning with Visual Tempo Consistency. <http://arxiv.org/abs/2006.15489> arXiv:2006.15489 [cs].
- [68] Haosen Yang, Deng Huang, Bin Wen, Jiannan Wu, Hongxun Yao, Yi Jiang, Xiatian Zhu, and Zehuan Yuan. 2022. Self-supervised Video Representation Learning with Motion-Aware Masked Autoencoders. <https://doi.org/10.48550/arXiv.2210.04154> arXiv:2210.04154 [cs].
- [69] Ting Yao, Yiheng Zhang, Zhaofan Qiu, Yingwei Pan, and Tao Mei. 2021. Seco: Exploring sequence supervision for unsupervised representation learning. In *Proceedings of the AAAI Conference on Artificial Intelligence*, Vol. 35. 10656–10664.
- [70] Yang You, Igor Gitman, and Boris Ginsburg. 2017. Large batch training of convolutional networks. *arXiv preprint arXiv:1708.03888* (2017).
- [71] Jure Zbontar, Li Jing, Ishan Misra, Yann LeCun, and Stéphane Deny. 2021. Barlow Twins: Self-Supervised Learning via Redundancy Reduction. In *Proceedings of the 38th International Conference on Machine Learning*. PMLR, 12310–12320. <https://proceedings.mlr.press/v139/zbontar21a.html> ISSN: 2640-3498.

## APPENDIX

The appendix provides supplementary material and additional details to support the main findings and methods. It is organized into several sections:

- Section A provides the pseudo code of our proposed BOLD-DI.
- Section B lists the definitions for all notations from the main text.
- Section C briefly introduces the recent approaches regarding the Koopman Operator theory.
- Section D provides a more detailed definition of the backdoor adjustment from the causal inference.
- Section E provides more ablation studies on the bi-level optimization problem, including different implementation methods and the number of the iterations of inner loop.
- Section F provides ablation studies regarding the choice of hyperparameters.
- Section G provides ablation studies on the impact of different components of BOLD-DI.
- Section H provides the evaluation performance of BOLD-DI on the downstream task of action detection on the AVA dataset.
- Section I provides the full results of Table 1 from the main text.

### A THE PSEUDO CODE FOR BOLD-DI

The pseudo code of BOLD-DI is illustrated below. The detailed implementation of Pytorch is provided in supplementary materials.

---

#### Algorithm 1 Pseudo Code of the proposed BOLD-DI

---

**Require:**  $f_{\theta}$  Networks

- 1: randomly initialize  $f_{\theta}$ .
- 2: **while** not converge **do**
- 3: Sample batch of videos  $\{X_i\}_{i=1}^N$ .
- 4: Sample  $\varrho$  clips  $\{X_i^{\rho}\}_{\rho=1}^{\varrho}$  for each video  $X_i$ .
- 5: **for** lower level update steps **do**
- 6: Get  $U_i^{\rho}, Z_i^{\rho}, Z_+, Z_-$  with  $f_{\theta}$ .
- 7: Get  $\mathcal{K}$  with Equation 5.
- 8: Perform eigenvalue decomposition of  $\hat{\mathcal{K}}$ .
- 9:  $\Phi_{dy} = []$ .
- 10: **for**  $\varphi_m$  in  $\Phi$  **do**
- 11:   **if**  $|\lambda_m| < \xi$  and  $\text{Arg}(\lambda_m) > \omega$  **then**
- 12:     Add  $\varphi_m$  to  $\Phi_{dy}$ .
- 13:   **end if**
- 14: **end for**
- 15:  $\mathcal{L}_{cl}(f_{\theta}, do) = 0$ .
- 16: **for**  $\varphi_j$  in  $\Phi_{dy}$  **do**
- 17:   Calculate  $P(X^+|X_i^{\rho}, \varphi_j)$  with Equation 11.
- 18:    $\mathcal{L}_{cl}(f_{\theta}, do) += -\log P(X^+|X_i^{\rho}, \varphi_j)$ .
- 19: **end for**
- 20: Update  $f_{\theta}^* \leftarrow f_{\theta} - \gamma \nabla_{f_{\theta}} \mathcal{L}_{cl}(f_{\theta}, do)$ .
- 21: **end for**
- 22: Get  $U_i^{\rho}, Z_i^{\rho}, Z_+, Z_-$  with  $f_{\theta}^*$ .
- 23: Calculate  $\mathcal{L}_{dynamic}(f_{\theta}^*)$  with Equation 6.
- 24: Calculate  $\mathcal{L}_{cl}(f_{\theta}^*)$  with Equation 1 or Equation 2.
- 25: Update  $f_{\theta} \leftarrow f_{\theta} - \gamma \nabla_{f_{\theta}} [\mathcal{L}_{cl}(f_{\theta}^*) + \nu \mathcal{L}_{dynamic}(f_{\theta}^*)]$
- 26: **end while**

---

## B TABLE OF NOTATIONS

We list the definitions of all notations from the main text in Table 6 and 7. Specifically, Table 6 contains the definition of notations from Section 3, while Table 7 contains the definition of notations from Section 4.

**Table 6: The definitions of all notations from Section 3.**

Notations	Definition
Notations of Subsection 3.1	
$\{X_i = \{x_{i,t}\}_{t=1}^T\}_{i=1}^N$	A mini-batch of videos.
$N$	The size of mini-batch.
$T$	The total number of frames.
$x_t \in \mathbb{R}^{H \times W \times C}$	A single frame
$H$	The height of the frame.
$W$	The width of the frame.
$C$	The channel of the frame.
$\rho_j, j \in \{1, \dots, \varrho\}$	The $j$ -th data augmentation.
$\varrho$	The number of data augmentations.
$L$	The length of the video clips.
$\delta$	The sampling stride when creating clips.
$f_{\theta}$	The spatiotemporal feature extractor.
$\theta$	The parameters of $f_{\theta}$ .
$\rho_j(X_i)$	The anchor sample.
$\rho_k(X_i),$ where $k \in \{1, \dots, \varrho\}, k \neq j$	The positive samples.
$f_{\theta}(\rho_j(X_i))$	The embeddings of anchor sample $\rho_j(X_i)$ .
$Z_+$	The set of embeddings of positive samples.
$Z_-$	The set of embeddings of negative samples.
$\ell_{i,j}^{\rho}$	The objective for clip $\rho_j(X_i)$ .
$\alpha$	The temperature hyper-parameter.
$f_{\theta_m}$	The target network.
$\theta_m$	The parameters of the target network.
$\gamma$	A hyper-parameter.
Notations of Section 3.3	
$X_i^{\rho}$	The video clips of the anchor sample.
$X^+$	The video clips of the positive sample.
$Z$	The embeddings of video clips.
$S$	The static semantics.
$D$	The dynamic semantics.

## C APPROACHES OF KOOPMAN OPERATOR THEORY

Nonlinearity is a central problem in dynamic systems [38]. Unlike linear systems, there is currently no mathematical framework for a general characterization of nonlinear systems. However, the Koopman operator theory [33] proves that the nonlinear dynamic of the system can be converted into an infinite-dimensional linear operator. Recently, Dynamic Mode Decomposition (DMD) [50] has become the standard algorithm to approximate the Koopman operator in a data-driven way. DMD has been widely applied to a diverse range of applications, such as fluid dynamics [50], neuroscience [6], and video processing [11]. Approximation of the Koopman operator utilizing deep neural networks has also gained increased attention in recent years [4, 39, 54].

**Table 7: The definitions of all notations from Section 4.**

Notations	Definition
Notations of Subsection 4.1	
$x_t$	The frame at time step $t$ .
$\mathcal{X}$	The space of video frames.
$F(x_t, t)$	The update rule for $x_t$ at time step $t$ .
$\mathcal{U}$	A infinite-dimensional space.
$\mathcal{G} : \mathcal{X} \rightarrow \mathcal{U}$	A nonlinear mapping from $\mathcal{X}$ to $\mathcal{U}$ .
$\mathcal{K}$	The Koopman operator.
$x_l$	The $l$ -th frame of the sampled video clip.
$u_l$	The representation of frame $x_l$ .
$X = [x_1, x_{1+\delta}, \dots, x_{1+(L-1)\delta}]$	The video clip.
$L$	The length of a video clip.
$\delta$	The sampling stride.
$U$	The set of representations of $X$ .
$\hat{\mathcal{K}}$	The estimated Koopman operator.
$X_{fore}$	The first $L - 1$ clips from $X$ .
$X_{back}$	The last $L - 1$ clips from $X$ .
$U_{fore}$	The representation of $X_{fore}$ .
$U_{back}$	The representation of $X_{back}$ .
Notations of Section 4.2	
$\Phi = [\varphi_1, \dots, \varphi_M] \in \mathbb{C}^{M \times M}$	The eigenvectors of $\mathcal{K}$ .
$\Lambda = \text{diag}([\lambda_1, \dots, \lambda_M]) \in \mathbb{C}^{M \times M}$	The diagonal matrix of eigenvalues of $\mathcal{K}$ .
$\mathbb{C}$	The set of all complex numbers.
$M$	The dimension of $\mathcal{K}$ .
$b = \Phi^{-1}\mathcal{G}(x_t)$	The projection of the frame $x_t$ .
$Re$	The real part of a complex number
$Im$	The imaginary part of a complex number
$Arg$	The argument of a complex number
$\text{atan2}$	The 2-argument arctangent function
$\xi$	An hyperparameter
$\omega$	An hyperparameter
Notations of Subsection 4.3 and 4.4	
$\varphi$	The eigenvector of $\mathcal{K}$
$Z_i^p$	The representation of $X_i^p$
$Z_t^p$	The representation of negative samples.
$J$	Number of dynamic semantics.
$\gamma$	The learning rate.

## D THE BACKDOOR ADJUSTMENT

We illustrate the derivation of Equation 3 by giving the following definitions from [20].

**DEFINITION 1.** (Path). A path consists of three components including the Chain Structure:  $A \rightarrow B \rightarrow C$ , the Collider Structure:  $A \rightarrow B \leftarrow C$  and the Fork Structure:  $A \leftarrow B \rightarrow C$ .

**DEFINITION 2.** ( $d$ -separation). A path  $p$  is blocked by a set of Nodes  $Z$  if and only if:

- $p$  contains a chain of nodes  $A \rightarrow B \rightarrow C$  or a fork  $A \leftarrow B \rightarrow C$  such that the middle node  $B$  is in  $Z$  (i.e.,  $B$  is conditioned on), or
- $p$  contains a collider  $A \rightarrow B \leftarrow C$  such that the collision node  $B$  is not in  $Z$ , and no descendant of  $B$  is in  $Z$ .

If  $Z$  blocks every path between two nodes  $X$  and  $Y$ , then  $X$  and  $Y$  are  $d$ -separated.

**DEFINITION 3.** (Backdoor Criterion). Given an ordered pair of variables  $(X, Y)$  in a DAG  $G$ , a set of variables  $Z$  satisfies the backdoor criterion relative to  $(X, Y)$  if no node in  $Z$  is a descendant of  $X$ , and  $Z$  blocks every path between  $X$  and  $Y$  that contains an arrow into  $X$ .

If a set of variables of  $Z$  satisfies the backdoor criterion for  $X$  and  $Y$ , then the causal effect of  $X$  on  $Y$  is given by:

$$P(Y = y | do(X = x)) = \sum_z P(Y = y | X = x, Z = z) P(Z = z) \quad (15)$$

## E ABLATION STUDIES ON THE BI-LEVEL OPTIMIZATION

### E.1 The implementation of the bi-level optimization

Multilevel optimization (MLO) tackles nested optimization scenarios, where lower-level optimization problems constrain upper-level ones in a hierarchical manner. MLO serves as a unified mathematical framework for various applications, including meta-learning [17, 45], neural architecture search [36], and reinforcement learning [46]. Numerous optimization algorithms have been proposed for solving MLO, with gradient-based approaches being particularly popular. These approaches leverage best-response Jacobians, computed using methods like iterative differentiation (ITD) or approximate implicit differentiation (AID), applying the chain rule. We implement our bi-level optimization algorithm using the *BETTY* library [9], designed for large-scale multilevel optimization (MLO). Specifically, we consider four MLO algorithms from *BETTY*, namely ITD-RMAD [17], AID-NMN [37], AID-CG [45], and AID-FD [36]. The details about these algorithms are as follows:

- **ITD-RMAD** [17] applies the implicit function theorem to the lower-level optimization problem and computes the gradients of the upper-level objective with respect to the upper-level parameters using reverse-mode automatic differentiation.
- **AID-NMN** [37] approximates the inverse of the Hessian matrix of the lower-level objective using a truncated Neumann series expansion and computes the gradients of the upper-level objective with respect to the upper-level parameters using forward-mode automatic differentiation.
- **AID-CG** [45] solves a linear system involving the Hessian matrix of the lower-level objective using the conjugate gradient algorithm and computes the gradients of the upper-level objective with respect to the upper-level parameters using forward-mode automatic differentiation.
- **AID-FD** [36] approximates the inverse of the Hessian matrix of the lower-level objective using a finite difference approximation and computes the gradients of the upper-level objective with respect to the upper-level parameters using forward-mode automatic differentiation.

### E.2 Ablation study on different implementations of bi-level optimization

We conduct an ablation study on different implementations of bi-level optimization. For all results in this section, the experiments are conducted with the Slow-R50 as the feature extractor, the video clip length  $L = 8$ , sampling stride  $\delta = 8$  and video resolution is set to  $224 \times 224$ , and the number of positive sample  $\rho = 2$ . For the evaluation of efficiency, the batch size is set to 3 and the experiments are conducted on a single NVIDIA V100 GPU. We evaluate four *BETTY* algorithms, namely ITD-RMAD [17], AID-NMN [37], AID-CG [45],

and AID-FD [36]. Table 8 compares the memory requirements and the time of each training iteration for each algorithm and also the baseline, namely the v-SimCLR.

**Table 8: Linear evaluation results of v-SimCLR+BOLD-DI on the Kinetics400 dataset with different BLO implementations.**

Implementation	Memory	Time/iter	Acc. (%)
v-SimCLR	4192MiB	2.2s	60.5
ITD-RMAD	5026MiB	3.1s	63.1
AID-NM	5134MiB	2.7s	62.8
AID-CG	5102MiB	2.9s	62.5
AID-FD	<b>4808MiB</b>	2.6s	<b>63.7</b>

As the results in Table 8 show, all methods with v-SimCLR+BOLD-DI outperform the original v-SimCLR method. Additionally, among the four MLO algorithms, the AID-FD has the shortest training duration while also the best performance on linear evaluation of Kinetics400. Therefore, the default setting of the implementation of bi-level optimization is set to AID-FD.

### E.3 Ablation study on the number of iterations in inner-loop

Our proposed BOLD-DI is a bi-level optimization procedure. The number of inner-loop update steps can significantly affect both the training duration and the performance. We present both the training time per iteration and the performance of linear evaluation on Kinetics 400, all experimental results following the standard experimental setting in Subsection 5.1. The results are illustrated in Table 9.

**Table 9: The comparison results on different inner-loop steps. In the table, the time consumption of each training iteration and the linear evaluation accuracy on Kinetics 400 are provided.**

Inner-loop steps	Time/iter	Acc. (%)
1	<b>2.6s</b>	63.7
5	4.7s	63.9
10	7.3s	<b>64.0</b>

As the results in Table 9 show, we can observe that, as the number of inner-loop steps increases, the time consumption of the training iteration also significantly increases. Specifically, when each inner-loop is updated for 10 steps, the training iteration time is almost three times the time consumption of just one inner-loop step, while the linear evaluation accuracy on the Kinetics 400 dataset increases by only 0.3%. Therefore, for training efficiency, we use only one inner-loop step by default.

## F ABLATION STUDIES ON HYPERPARAMETERS

**Ablation study on  $\nu$ .** As we mentioned in Subsection 4.4.  $\nu$  is a hyperparameter that determine the impact of the loss  $\mathcal{L}_{dynamic}(f_{\theta}^*)$ .

We present the results of different choices of  $\nu$  in Table 10. All results are linear evaluation results on Kinetics400 based on v-SimCLR + BOLD-DI, with the default experimental setting in Subsection 5.1, and number of positive samples  $\varrho = 2$ .

**Table 10: The comparison results on different choices of the hyperparameter  $\nu$ . All results are linear evaluation results with v-SimCLR + BOLD-DI on Kinetics400.**

$\nu$	$10^{-3}$	$10^{-2}$	$10^{-1}$	1	$10^1$	$10^2$	$10^3$
Acc.(%)	62.8	63.4	<b>63.7</b>	63.6	63.4	63.4	63.1

The choice of  $\nu$  determines the role of  $\mathcal{L}_{dynamic}(f_{\theta}^*)$  in the overall objective in Equation 12. From the results in Table 10, we can observe that the linear evaluation performance initially increases and subsequently decreases, with the optimal choice of  $\nu$  being approximately  $10^{-1}$ .

**Ablation study on  $\xi$ .** As we mentioned in Subsection 4.2. The hyperparameter  $\xi$  should enable the Stratify Module to effectively separate the static semantics from the dynamic semantics. Specifically,  $\xi$  is a threshold of the magnitude of the eigenvalues, eigenvalues with a larger magnitude than  $\xi$  can be considered as related to static semantics. We present the results of different choices of  $\xi$  in Table 11. All results are linear evaluation results on Kinetics400 based on v-SimCLR + BOLD-DI, with the default experimental setting in Subsection 5.1, and number of positive samples  $\varrho = 2$ , the default argument threshold  $\omega = 0.1$ .

**Table 11: The comparison results on different choices of the hyperparameter  $\xi$ . All results are linear evaluation results with v-SimCLR + BOLD-DI on Kinetics400. The default  $\omega$  is 0.1.**

$\xi$	0.6	0.7	0.8	0.9	0.99
Acc.(%)	62.3	62.6	63.1	<b>63.7</b>	63.5

From the results in Table 11, we can observe that when the value of  $\xi$  is closer to 1, the linear evaluation accuracy of the v-SimCLR + BOLD-DI also increases. However, when the  $\xi$  is set too close to 1, the performance slightly decreases. We hypothesize that it is because in videos, most semantics, including the background, are slowly moved, therefore, to effectively separate the static semantics from the dynamic semantics,  $\xi$  should not be set too close to 1.

**Ablation study on  $\omega$ .** As we mentioned in Subsection 4.2.  $\omega$  is the threshold of the argument of the eigenvalues, eigenvalues with a smaller argument than  $\omega$  can be considered as related to static semantics. We present the results of different choices of  $\omega$  in Table 12. All results are linear evaluation results on Kinetics400 based on v-SimCLR + BOLD-DI, with the default experimental setting in Subsection 5.1, and number of positive samples  $\varrho = 2$ .

The value of  $\omega$  lies between  $-\pi$  to  $\pi$  according to the definition of the cosine function. As shown in Table 12, the linear evaluation performance improves as the value of  $\omega$  approaches 0. However, similar to the phenomenon observed during in ablation of  $\xi$ , a threshold that is set too close to 0 also slightly hurts the performance

**Table 12: The comparison results on different choices of the hyperparameter  $\omega$ . All results are linear evaluation results with v-SimCLR + BOLD-DI on Kinetics400. The default  $\xi$  is 0.9.**

$\xi$	0.01	0.1	0.2	0.3	0.5
Acc.(%)	63.5	<b>63.7</b>	63.4	63.1	62.7

of v-SimCLR + BOLD-DI. Consequently, the default value for  $\omega$  is set at 0.1.

**Ablation study on  $M$ .** As we mentioned in Subsection 4.2,  $M$  is the total number of eigenvectors and also the dimension of the estimated Koopman operator  $\hat{\mathcal{K}}$ . Different choices of  $M$  might influence how much dynamic semantics the Stratify module can obtain. We provide an ablation study on this hyperparameter in Table 13. All results are linear evaluation results on Kinetics400 based on v-SimCLR + BOLD-DI with the default experimental setting in Subsection 5.1.

**Table 13: The comparison results on different choices of the number of eigenvectors  $M$ . The results are linear evaluation on Kinetics400 with v-SimCLR + BOLD-DI.**

$M$	16	32	64	128	256	512
Acc.(%)	62.3	62.5	62.8	<b>63.7</b>	63.6	63.7

From the results in Table 13, we can observe that as  $M$  increases, the performance on Kinetic400 first increases and then stays stable afterward. This indicates that the optimal choice of  $M$  should be 128 because further increasing  $M$  can lead to more memory requirements.

## G ABLATION STUDIES ON COMPONENTS OF BOLD-DI

In this section, we investigate different components of the objective of BOLD-DI, i.e. the Equation 12. Specifically, we present the linear evaluation performance of v-SimCLR, v-SimCLR +  $\mathcal{L}_{dynamic}$ , v-SimCLR +  $\mathcal{L}_{f_{\theta},do}$  on Kinetics400, the fine-tune performance on UCF-101 and HMDB-51, with the default setting in Subsection 5.1. Note that the results of v-SimCLR +  $\mathcal{L}_{dynamic}$  didn't require bi-level optimization, while the results of v-SimCLR +  $\mathcal{L}_{f_{\theta},do}$  require bi-level optimization.

Method	K400	UCF-101	HMDB-51
v-SimCLR	60.5	88.9	67.2
v-SimCLR + $\mathcal{L}_{dynamic}$	61.2	89.7	69.2
v-SimCLR + $\mathcal{L}_{f_{\theta},do}$	61.1	89.5	68.4
v-SimCLR + BOLD-DI	<b>63.7</b>	<b>90.2</b>	<b>70.6</b>

**Table 14: Comparison results for linear evaluation on Kinetics400 and fine-tuning on UCF-101 and HMDB-51, with different components of BOLD-DI.**

From the results in Table 14, we can observe that both v-SimCLR +  $\mathcal{L}_{dynamic}$ , v-SimCLR +  $\mathcal{L}_{f_{\theta},do}$  perform better than v-SimCLR alone. However, the performance of v-SimCLR + BOLD-DI, which combines these two components, significantly outperforms not only the original v-SimCLR but also the performance of either component in isolation. These results validate the correctness of our analysis presented in the main text.

## H ACTION DETECTION

**Dataset** We evaluate the performance of BOLD-DI on the AVA [23] dataset, which is an action detection dataset taken from 437 movies, with bounding box annotations for spatiotemporal localization of human actions.

**Implementation and evaluation protocol.** We follow the standard protocol [13, 14] to train a detector that is similar to Faster R-CNN [48] with minimal modifications adapted for video. The pre-trained network  $f_{\theta}$  is used as the backbone. The region-of-interest (RoI) features [18] are extracted at the last layers of the backbone network, and extend into 3D by replicating it along the temporal axis. The region proposals are computed with an off-the-shelf person detector, which is pre-trained with Detectron [19]. We report the detection performance with mean Average Precision (mAP) over 60 classes with a frame-level IoU threshold of 0.5.

**Table 15: Action detection results on AVA datasets**

Method	mAP	(+BOLD-DI)
v-SimCLR	17.6	21.4 ( $\uparrow$ 3.8)
v-BYOL	23.4	<b>26.3</b> ( $\uparrow$ 2.9)
v-MoCo	20.3	23.2 ( $\uparrow$ 2.9)
v-SwAV	18.2	21.4 ( $\uparrow$ 3.2)

**Results** The results of action detection is illustrated in Table 15. From the results, our proposed BOLD-DI improved the performance of v-CLs by an average of 3.2%. These results demonstrate that the representations learned through our method enable the detector to better capture the information of physical entities and to detect the types of action. This suggests that our model has learned to capture both dynamic and static semantics.

## I FULL RESULTS

We present the full results of Table 1 from the main text. Specifically, comparing to Table 1 of the main text, the results in 16 contains also the comparison results when using R(2+1)D-18 [59] and S3D-G [66] as the feature extractor.

**Table 16: Finetuning Results (average of 3 splits) for action classification on UCF101 and HMDB51. Self-supervised pretraining is done on Kinetics 400 datasets. All results without special notations are from the original article. Results with "†" are reproduced according to the open-source repositories. Results with "\*" utilize the ImageNet1K pre-trained weight. "-" means not mentioned in the original paper. As for modality, "V" indicates RGB video, "A" indicates audio, and "F" indicates optical flow.  $\rho$  is the number of positive samples.**

Method	Resolution	Frames	Architecture	Param.	Epochs	Modality	UCF101	HMDB51
SpeedNet [2]	224×224	16	S3D-G	9.1M	-	V	81.1	48.8
CoCLR [24]	128×128	16	S3D-G	9.1M	300	V + F	90.6	62.9
v-BYOL $_{\rho=4}^{\dagger}$	112×112	16	S3D-G	9.1M	200	V	87.8	69.8
v-BYOL $_{\rho=4}$ + BOLD-DI	112×112	16	S3D-G	9.1M	200	V	<b>91.1 († 3.3)</b>	<b>71.6 († 1.8)</b>
VTHCL [67]	224×224	8	R3D-18	13.5M	200	V	80.6	48.6
TCLR [10]	112×112	16	R3D-18	13.5M	100	V	85.4	55.4
VideoMoCo [41]	112×112	16	R3D-18	13.5M	200	V	74.1	43.6
SLIC [32]	128×128	32	R3D-18	13.5M	150	V	83.2	52.2
MACLR [65]	112×112	32	R3D-18	13.5M	600	V	91.3	62.1
v-BYOL $_{\rho=4}^{\dagger}$	112×112	16	R3D-18	13.5M	200	V	88.3	69.3
v-BYOL $_{\rho=4}$ + BOLD-DI	112×112	16	R3D-18	13.5M	200	V	<b>92.3 († 3.5)</b>	<b>71.1 († 1.8)</b>
PacePred [63]	112×112	16	R(2+1)D-18	15.4M	18	V	77.1	36.6
PacePred $^{\dagger}$ [63]	112×112	16	R(2+1)D-18	15.4M	200	V	84.3	55.2
VideoMoCo [41]	112×112	16	R(2+1)D-18	15.4M	200	V	78.7	49.2
TCLR [10]	112×112	16	R(2+1)D-18	15.4M	100	V	88.2	60.0
TCLR $^{\dagger}$	112×112	16	R(2+1)D-18	15.4M	200	V	90.8	64.3
GDT [42]	112×112	32	R(2+1)D-18	15.4M	200	V + A	89.3	60.0
v-BYOL $_{\rho=4}^{\dagger}$	112×112	16	R(2+1)D-18	15.4M	200	V	90.1	69.4
v-BYOL $_{\rho=4}$ + BOLD-DI	112×112	16	R(2+1)D-18	15.4M	200	V	<b>92.9 († 1.8)</b>	<b>72.4 († 3.0)</b>
SeCo [69]	112×112	50	R50+TSN	25M	400	V	88.3	55.6
DSM [61]	112×112	16	C3D	27.7M	200	V	70.3	40.5
CVRL [44]	224×224	32	R3D-50	31.8M	800	V	92.2	66.7
MACLR [65]	224×224	32	R3D-50	31.8M	600	V	94.0	67.4
MACLR [65]	224×224	32	R3D-50	31.8M	600	V + F	94.2	67.2
v-SimCLR $_{\rho=2}$ [14]	224×224	8	R3D-50	31.8M	200	V	88.9	67.2 $^{\dagger}$
v-SwAV $_{\rho=2}$ [14]	224×224	8	R3D-50	31.8M	200	V	87.3	68.3 $^{\dagger}$
v-MoCo $_{\rho=4}$ [14]	224×224	8	R3D-50	31.8M	200	V	93.5	71.6 $^{\dagger}$
v-BYOL $_{\rho=4}$ [14]	224×224	8	R3D-50	31.8M	200	V	94.2	72.1
v-BYOL $_{\rho=4}$ [14]	224×224	16	R3D-50	31.8M	200	V	95.5	73.6
v-SimCLR $_{\rho=2}$ + BOLD-DI	224×224	8	R3D-50	31.8M	200	V	90.2 († 1.3)	70.6 († 3.4)
v-SwAV $_{\rho=2}$ + BOLD-DI	224×224	8	R3D-50	31.8M	200	V	92.2 († 4.9)	73.3 († 5.0)
v-MoCo $_{\rho=4}$ + BOLD-DI	224×224	8	R3D-50	31.8M	200	V	94.4 († 0.9)	75.2 († 3.6)
v-BYOL $_{\rho=4}$ + BOLD-DI	224×224	8	R3D-50	31.8M	200	V	95.1 († 0.9)	74.6 († 2.5)
v-BYOL $_{\rho=4}$ + BOLD-DI	224×224	16	R3D-50	31.8M	200	V	<b>96.5 († 1.0)</b>	<b>75.8 († 2.2)</b>
VideoMAE [58]	224×224	16	ViT-B	87M	800	V	96.1	73.3
MotionMAE [68]	224×224	16	ViT-B	87M	800	V	96.1	73.3
MME [53]	224×224	16	ViT-B	87M	800	V	96.5	78.0
MGM [12]	224×224	16	ViT-B	87M	800	V	91.9	69.7
v-BYOL $_{\rho=4}^{\dagger}$	224×224	16	ViT-B	87M	800	V	95.2	76.8
v-BYOL $_{\rho=4}$ + BOLD-DI	224×224	16	ViT-B	87M	800	V	<b>96.9 († 1.7)</b>	<b>78.2 († 1.4)</b>